Chapter 1

General Introduction

This chapter presents the motivation for this PhD project and a general introduction to two-dimensional (2D) materials, namely graphene and transition metal dichalcogenides (TMDs), with a major focus on molybdenum disulfide (MoS_2). The crystal structure, electronic and optical properties of MoS_2 are also discussed. Several types of defects present in MoS_2 are explained both from the theoretical and the experimental point of view, followed by a summary on tailoring MoS_2 properties via surface functionalization. In the last section, the outline of the thesis is provided.

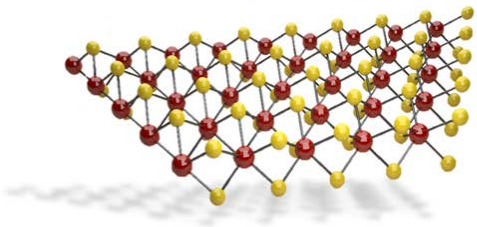

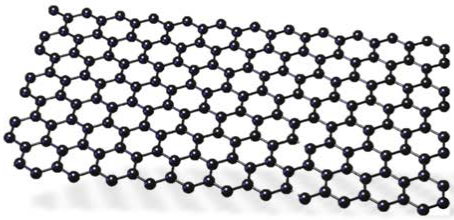

1.1 Motivation

'*What is next?*' is a common phrase addressed to scientists trying to find a promising candidate for substituting silicon in the electronics industry. Silicon, the second most abundant resource in our planet's crust, has been used to make transistors, the smallest component in electronic devices. The first type of transistor, the field effect transistor invented in 1925 by Julius Edgar Lilienfeld,[1] consists of three terminals; source, drain, and gate. The current flowing from the source to the drain is controlled by the gate voltage. The open gate allows electrons to flow - the 1 state, while the closed gate means where no electrons are flowing, represents the 0 state.

An electronic device comprises billions of transistors. As devices get smaller, they perform faster and consume less power. Gordon Moore, Intel *Co-Founder*, predicted the development for transistors known as the Moore's law: "*the number of transistors incorporated in a chip approximately doubles every 24 months*".[2] However, this law is expected to end in the next 6 years because Si-based components cannot be made any smaller due to quantum effects.

Shrinking down a transistor means scaling down all parts including the gate. The most recent chip made by Intel has gate length of 14 nm. This size is 5000 times smaller than the diameter of human hair. However, when the gate gets smaller, typically below 5 nm, it is no longer able to stop the electron from flowing from the source to the drain. This means that the transistor cannot be turned off. Consequently, the search for new materials that can replace Si has already started.

In this regard, graphene, a two-dimensional (2D) allotrope of carbon consisting of one single layer of atoms offers much hope. Graphene's era started in 2004 when a field effect transistor made of graphene performed outstandingly.[3] The carrier mobility in graphene-based devices has been found to be six order of magnitude higher than in copper. Not only that, graphene is also an excellent heat conductor, it is transparent, robust and bendable and hence an excellent candidate for flexible electronic devices.[4] On the other hand, graphene is a gapless semiconductor, which hinders its utilization in a transistor application since it cannot be turned off.

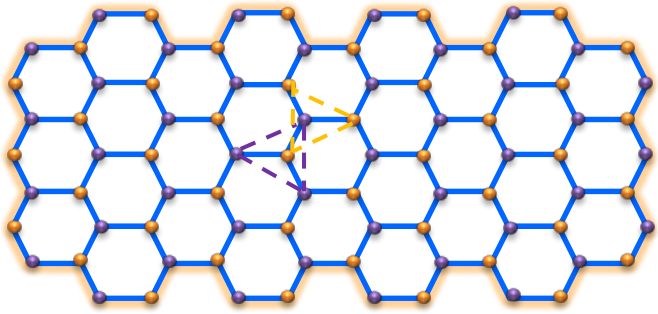

Figure 1.1. *Honeycomb structure of graphene consisting of two interpenetrating triangular sub-lattices (represented by different colours).*

Some efforts have been made to open up a band gap via chemical modification[5] and physisorption of molecules.[6] However, such additional processes make the inclusion of graphene in the device fabrication procedure more complicated.

The birth of graphene triggered the research community to find other prospective materials that can be applied in electronic devices. Transition metal dichalcogenides (TMDs) constitute a vast family of layered materials with diverse electronic properties. Among all TMDs, molybdenum disulfide (MoS_2) has been the most studied 2D material due to its unique electronic properties suitable for a plethora of applications including transistors, sensors and photodetectors.[7–9]

The primary objective in this PhD project was to explore the properties of two 2D materials, MoS_2 and graphene. In the case of graphene, the wetting and anti-icing properties were investigated, while for MoS_2 we focussed on how to optimize the growth for obtaining large single crystalline grains and on how to control the electronic properties by molecular doping. In the next sections, we present a general introduction to graphene and MoS_2.

1.2 Graphene

Graphene is a two-dimensional (2D) allotrope of carbon with a honeycomb structure. It consists of two interpenetrating triangular sub-lattices as illustrated in ***Figure 1.1***. Carbon atoms from a specific lattice (*i.e.* lattice A) are at the center of the

triangle formed by atoms of the other lattice (lattice B). The concept of graphene has been known since the early 1940s when it was introduced as a first step to describe complex systems of aromatic carbon; the single layer of graphitic carbon was used to calculate the band diagram and predict the electrical properties.[10] However, the milestone in graphene research was when A. Geim and K. Novoselov fabricated a graphene-based field effect transistor in 2004, a work which afforded them the Nobel prize six years later.[3]

Graphene is considered as the mother of other carbon allotropes as sketched in ***Figure 1.2.*** When many graphene layers stacked together through Van der Waals (VdW) interaction, they will form graphite, one of the three-dimensional (3D) carbon allotropes. Under certain conditions, single or multi-layers of graphene can be rolled in a particular direction to form a carbon nanotube (CNT), the one-dimensional (1D) carbon allotrope.[11,12] Lastly, when graphene is wrapped into a spherical shape by the introduction of pentagons, fullerene, a zero-dimensional (0D) carbon allotrope[13] is formed.

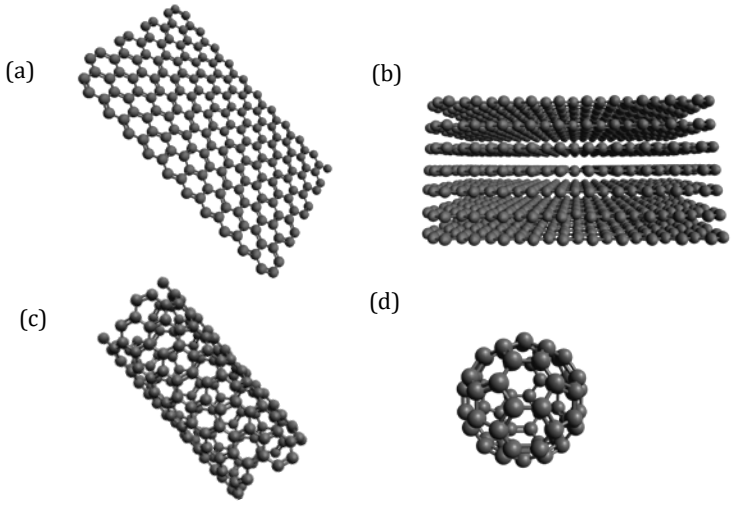

Figure 1.2. *Graphene as the mother of other carbon allotropes* ***(a)*** *Graphene (2D),* ***(b)*** *Graphite (stacked graphene, 3D),* ***(c)*** *carbon nanotubes (rolled-up graphene,1D), (d) fullerene (wrapped-up graphene, 0D)*

As mentioned above, graphene was successfully mechanically exfoliated from its bulk form of graphite by a well-known scotch tape method.[3] The one-atom thick layer of graphene is known to be the thinnest material with exceptional electrical and thermal conductivity. Its zero-band gap allows the electron to flow as a massless particle, resulting in an excellent carrier mobility up to $10^5\ cm^2/V.s$.[4]. Graphene is not only flexible, highly transparent but also has high tensile strength, which makes it stronger than steel or even diamond.

The extraordinary properties of graphene can be exploited in applications such as electronic devices, solar cells, sensors, anti-bacterial and anti-corrosion coatings.[14–16] More than 50.000 papers were published until 2016,[17,18] spanning from various synthesis methods to exploring the mechanical, thermal, optical and electrical properties as well as to applications in electronic devices, gas storage, batteries, coating, sensors and the water treatment.[15,19–24]

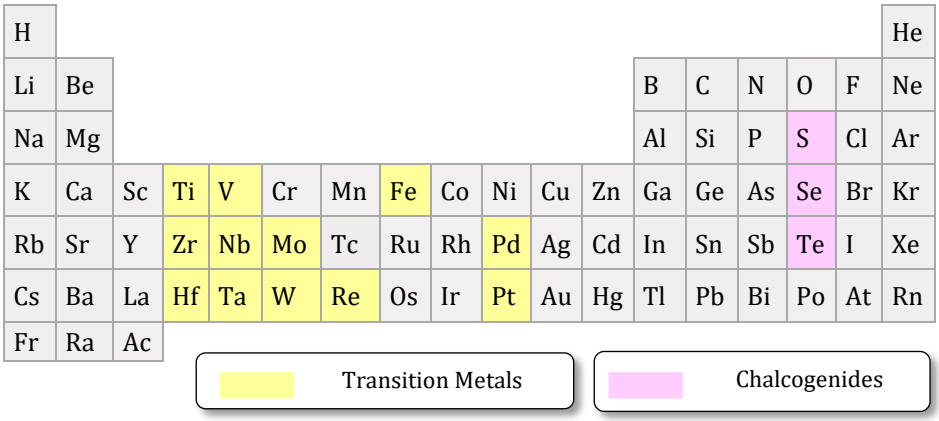

Figure 1.3. *Periodic table the transition metals and chalcogen atoms that compose the TMDs family. The metals from groups 4-7 give rise to layered structures, while Fe, Pd and Pt form non-layered TMD structures.* [25]

1.3 Transition Metal Dichalcogenides

Despite the excellent properties of graphene, as already mentioned, it presents a significant disadvantage when it comes to application in electronic devices: it has no band gap. Due to that reason, many scientists' attention shifted to other layered materials such as transition metal oxide, hexagonal boron nitride (hBN) and transition metal dichalcogenides (TMDs).[26–29] TMDs are particularly attractive because they comprise a significant number of compounds with different electronic properties, for example MoS_2, $MoSe_2$, WSe_2, WSe_2 are semiconducting, $MoTe_2$ is metallic and $NbSe_2$ superconducting. These different characteristics stem from the variation in hybridization of the transition metal *d* orbital and the chalcogen *p* orbital.[30] ***Figure 1.3*** shows the periodic table highlighting the transition metal and chalcogen atoms giving rise to stable TMDs.[31]

Layered TMDs, symbolized by MX_2, consist of a sheet of transition metal (M) atoms of group 4, 5, 6 or 7, sandwiched between two chalcogen (X) layers. This tri-layer structure can be stacked into a solid held together by Van der Waals (VdW) forces. The VdW interaction enables the tri-layers to be isolated in the 2D form by mechanical cleavage. In addition, VdW interaction is responsible for the TMDs' shearing properties, which qualify them as solid lubricants.

Among all the TMDs, molybdenum disulfide (MoS_2) has been the most studied material due to its remarkable optical and electronic properties.[32–35] In contrast to graphene, atomically thin MoS_2 is a semiconductor with a modest band gap of 1.29 eV, suitable for nanoelectronic applications. Furthermore, some promising results have been obtained application of MoS_2 in the fields of the hydrogen evolution reaction (HER), energy conversion in solar cells, and desalination of water.[23,36,37]

1.4 Molybdenum disulfide (MoS_2)

1.4.1 Crystal Structure

Bulk MoS_2 occurs in different polymorphs depending on the stacking alignment of the S and Mo atoms in the S-Mo-S layers, namely 2*H* and 3*R*-MoS_2; the digit indicates the number of S-Mo-S layers, while the letter stands for hexagonal and rhombohedral. The 2*H*-MoS_2 stacks ABAB whereas 3*R*-MoS_2 follows an ABCABC arrangement.

Single layer (SL) MoS_2 is a three-atom thick nanosheets with a thickness around 6~8 Å. Based on the Mo coordination, SL-MoS_2 can have two different phases, 2*H*-MoS_2 or 1*T*-MoS_2. In 2*H*-MoS_2 Mo has a trigonal prismatic coordination with a hexagonal symmetry (D_{3h} group), while in 1*T*-MoS_2 phase Mo has octahedral coordination with a tetragonal symmetry (D_{3d} group). S-Mo-S arranges with ABA stacking in 2*H*-MoS_2, meaning that both S atoms have the same position along the z-axis. In contrast, the second S atom is shifted in the case of 1*T*-MoS_2, which stacks in a ABC sequence as depicted in ***Figure 1.4***.

The Mo coordination and the *d*-orbital filling determine the electronic properties of SL-MoS_2; 2*H*-MoS_2 is semiconducting and and 1*T*-MoS_2 metallic. In the trigonal prismatic coordination, the *d* orbital of Mo atom has 3 degenerate states, d_{z^2} (a_1), $d_{x^2-y^2,xy}$(e) and $d_{xz,yz}$ (e'), while in the octahedral coordination it splits into 2 states, d_{z^2,x^2-y^2} (e_g) and $d_{xy,xz,yz}$ (t_{2g}).[38] The different polymorphs of MoS_2 as well as the splitting *d*-orbital of Mo atom are illustrated in ***Figure 1.4***. In this thesis, we only focus on the semiconducting 2*H*-MoS_2 phase, which will be written as MoS_2 for simplicity.

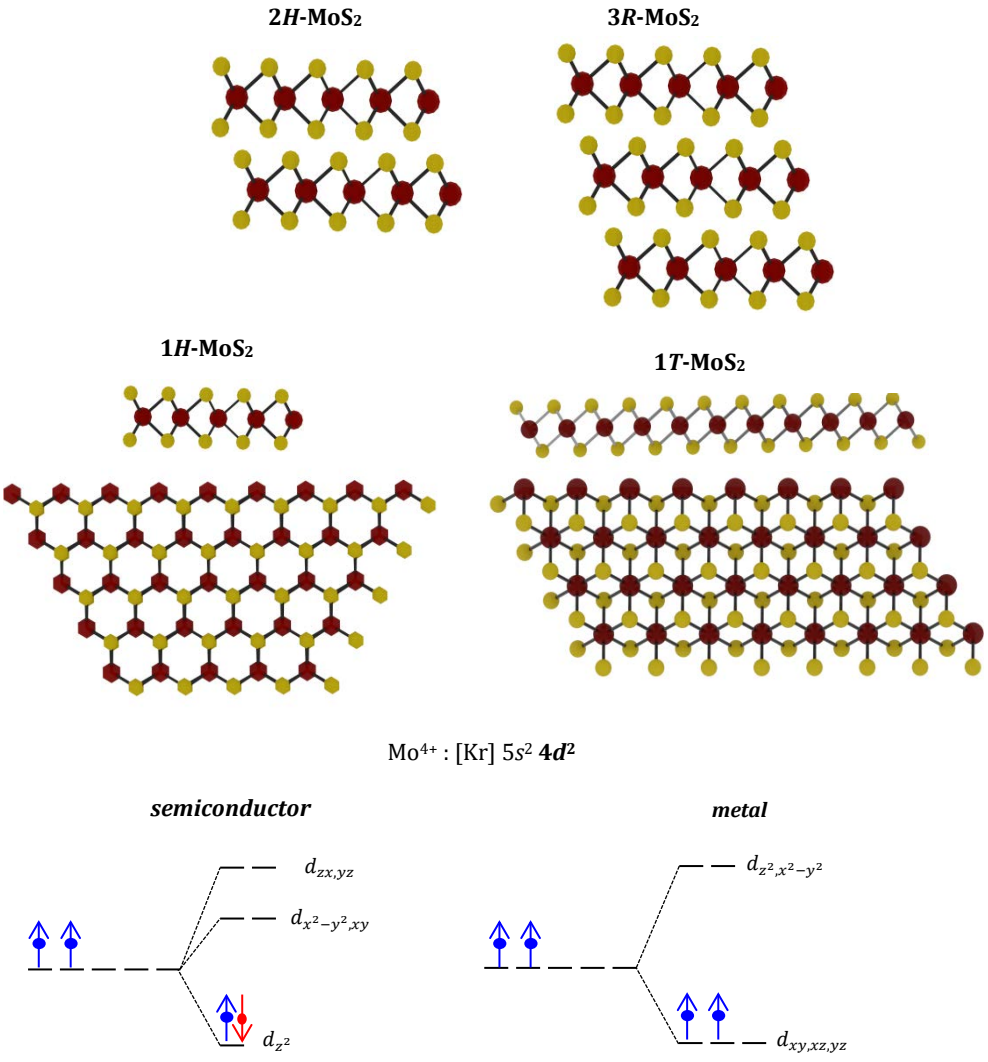

Figure 1.4. *Schematic illustration of different polymorphs of MoS_2 namely 1T-MoS_2, 2H-MoS_2 and 3R-MoS_2 and the d-orbital splitting in Mo atom, which determines MoS_2 electronic characteristics*

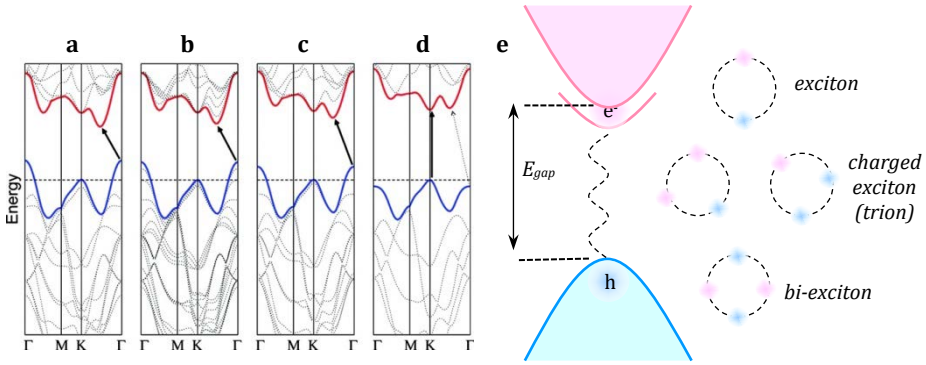

Figure 1.5. *The density functional theory (DFT) calculation of the band diagram of* ***(a)*** *bulk,* ***(b)*** *quadlayers,* ***(c)*** *bilayers,* ***(d)*** *monolayer MoS_2.[39] The red and blue line indicates the CBM and VBM, respectively, the solid black arrow indicates the lowest transition while the dash arrow in the monolayer MoS_2 indicates the indirect transition.* ***(e)*** *Schematic illustration of excitonic recombination and more complex quasiparticles; trion and bi-exciton.*[40]

1.4.2 Electronic and Optical Properties

Bulk MoS_2 is a semiconductor with the conduction band minimum (CBM) located between the K and Γ points and valence band maximum (VBM) at the Γ point.[41–43] It has an indirect band gap of 1.29 eV, but when the thickness is reduced, the indirect band gap drastically increases due to quantum confinement effects in the out-of-plane direction, as illustrated in the DFT calculation reproduced in ***Figure 1.5(a-d)***[41], resulting for SL-MoS_2 in a 1.89 eV direct band gap located at K and K'.[42] The calculation confirms that the band around the Fermi level is mainly derived from the strong hybridization between the *d* orbital of Mo atom and the *p* orbital of the S atom. These results also show that the interlayer interaction is more affected at the Γ point, resulting in a blue-shift of the indirect band gap due to the hybridization between the *d* orbital of Mo atom and the p_z antibonding orbital of S atom, while the direct band gap at the K point remains the same.

The band gap between VBM and CBM can be probed experimentally by either optical[44] or transport[45] measurements, which result in slightly different values. The obtained band gap from transport measurements is called electronic band gap and corresponds to the situation where an electron is knocked out and a hole in the valence band is created. The process involves a decrease in the total number of charge carriers

in the material. The band gap obtained from optical measurements refers to the case when a photon (in direct process; $\hbar\upsilon > E_g$) creates an exciton, a bound state between an electron in the energy state below the conduction band and a hole in the valence band, which interact via Coulomb interaction.[40] The optical transition does not alter the number of charge carriers in the material. The energy difference between the electronic and optical band gap is therefore a measure of the strength of the Coulomb interaction between electron and hole, also defined as the binding energy of the exciton.[39,42] The electronic band gap is generally 200-400 meV larger than the optical band gap.[46–48] In addition, the strong binding energy of the exciton allows the observation of other quasiparticles in the form of charged exciton (bound state of an exciton with an electron or a hole) and bi-exciton (bound state of two exciton) at room temperature[49,50] as depicted in ***Figure 1.5(e).***

1.4.3 Defects and defect engineering in MoS_2

The term defect in 2D materials refers to adatoms, wrinkles, grain boundaries, edges and vacancies. Vacancies are the most common defect observed in MoS_2 irrespective of preparation method, be it by mechanical cleavage, chemical exfoliation, liquid exfoliation or chemical vapour deposition (CVD).[51–54] Theoretical and experimental studies have shown that vacancies are responsible for decreasing the photoluminescence (PL) intensity as well as for reducing the mobility in MoS_2 based transistors.[55,56] Therefore, understanding their role is crucial to tune the electronic properties of MoS_2 in a more controllable fashion.

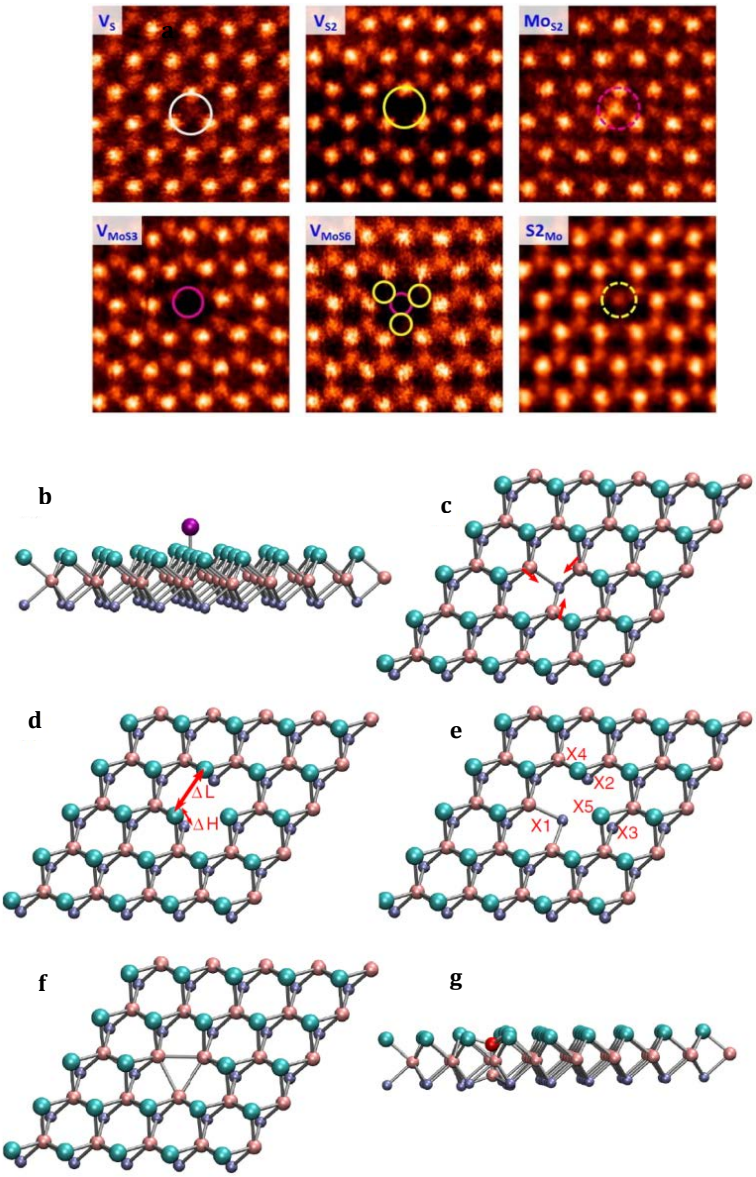

Figure 1.7(a) *Various types of defects present in CVD grown MoS_2 as seen by scanning transmission electron microscopy.* [57] *Illustration of different structural defects calculated by density functional theory* ***(b)*** *adatom at S column,* ***(c)*** *S vacancy,* ***(d)*** *Mo vacancy,* ***(e)*** *MoS divacancies,* ***(f)*** *SS divacancies,* ***(g)*** *adatom at interstitial site.* [58]

From the application point of view, one can utilize the defect density in order to tailor the electronic properties of MoS_2. Zhou *et al.* [57] reported direct evidence for the presence of various types of defects in CVD grown MoS_2 by using Scanning Transmission Electron Microscopy (STEM). The authors identified the monosulfur vacancy (V_S), disulfur vacancies (V_{S2}), as well as complex vacancies, where one Mo atom and three S atoms are missing (V_{MoS3}) or one Mo atom and six S atoms are missing (V_{MoS6}), or anti-site defects, where a Mo atom substitutes for a S2 column (Mo_{S2}) or an S2 column substitutes a Mo atom ($S2_{Mo}$), as depicted in ***Figure 1.7(a)***. By combining their observations with Density Functional Theory (DFT) calculation, they confirmed the relation between the defects and the electronic properties of MoS_2. A theoretical study by Soumyajyoti *et al.*[58] supports this work. These authors classified the defects based on their stability, and determined the formation energy in different growth condition. They also investigated the relation between the defects and the modification of the electronic and optical properties of defective TMDs including MoS_2.[58] The calculation identified some stable defects including S vacancies, Mo vacancies, S and Mo divacancies consisting of either two S atoms or a MoS pair, and an adatom at an interstitial site, as depicted in ***Figure 1.7(b-g)***. The existence of intrinsic defects in MoS_2 calls for protocols to not only heal the defects but also to functionalize the nanosheet in order to tune the physical and chemical properties.

The first attempt to functionalize MoS_2 have been reported by Chhowalla's group[59], who reacted bulk MoS_2 with *n*-butyllithium in hexane solution. The idea was to intercalate Li^+ ion between MoS_2 layers to weaken the interlayer interaction and increase the repulsive forces between the negatively charged MoS_2 sheets. Chemically exfoliated MoS_2 nanosheets were obtained by dispersion in water with the help of a mild sonication and the additional negative charges on the MoS_2 nanosheet exploited by reacting with strongly electrophilic molecules such as organic halides or diazonium salts to yield functionalized-MoS_2 with improved dispersibility.[60] The functionalization reaction using this approach involves a modification of the MoS_2 crystal structure from the 1H-MoS_2 to the 1T-MoS_2 phase. However, the semiconducting MoS_2 can be recovered by simply heating the 1T-MoS_2.

McDonald *et al.*[61] developed an approach to functionalize MoS_2 with $M(OAc)_2$ salts where M are Ni, Cu and Zn without yielding the 1T polytype by employing an exfoliation in a mild reaction using liquid phase exfoliation (LPE) in a 2-propanol (IPA) solution. The IPA-MoS_2 interaction allows the exfoliation with typically 9-10 nanosheets in the exfoliated flake. The functionalization takes place through the S atoms at the surface. Similarly, Coleman *et al.*[62] successfully prepared a MoS_2 dispersion in a water-based solution by adding the surfactant sodium cholate; the generated 2-9 layer thick nanoflake of MoS_2 remained dispersed for more than 25 days without re-aggregation due to the electrostatic repulsion.

Another exciting result has been obtained by Matsuda *et al.*[63] who demonstrated tunable PL spectra in functionalized-MoS_2 obtained by micromechanical exfoliation with the p-dopants 2,3,5,6-tetrafluoro-7,7,8,8-tetracyanoquinodimethane (F_4TNCQ) and 7,7,8,8-tetracyanoquinodimethane (TCNQ) and the n-dopant nicotinamide adenine dinucleotide (NADH). The adsorbed p-dopants can effectively enhance the PL intensity due to the suppression of trion recombination followed by an increase of exciton recombination. *Vice versa*, the n-dopant can reduce the PL intensity due to the injection of additional electron generating more trion recombination.

Most of the covalent functionalization of MoS_2 has been obtained by chemical exfoliation. Only few papers report on functionalization of CVD grown MoS_2 due to its naturally inert basal plane characteristics. One of the efforts has been made by Jin *et al.*[64] who functionalized CVD grown MoS_2 with 4-fluorobenzyl mercaptan. They revealed the role of sulfur vacancies as active sites for anchoring the molecules. The molecules partially healed the vacancies and thus enhanced the PL intensity and decreased the active sites for hydrogen evolution reaction (HER).

Understanding the role of defects is important to facilitate carrier transport, phase engineering, tuning the electronic band structure and to induce doping. Several studies have been reported in controlling MoS_2 electronic properties by either non-covalent or covalent surface functionalization via surface charge transfer mechanisms, which take advantage of the presence defects in the MoS_2 nanosheet.

The non-covalent functionalization allows reversible tuning of the electronic properties: the molecules merely physisorb on MoS_2 and can be easily removed by exposure to solvent.[65] On the other hand, the covalent functionalization represents a robust system where the S atom of a thiol-containing molecule binds directly to a Mo atom in the MoS_2 nanosheet[66]. Both methods give rise to new MoS_2 applications spanning from optoelectronics, catalysis, sensor, medical and water treatment.[23,36,67–70] ***Table 1.1.*** summarizes the modification of electronic properties of MoS_2 via surface functionalization using different molecular dopants. The n- or p-type doping is achieved through the functional group attached to the molecules.

Table 1.1. *Studies of molecular doping of* MoS_2 [59,63,65,71–81]

Preparation method	Adsorbed molecule	Type of adsorption	Result	Ref.
Mechanical Exfoliation	Triphenylphosphine (PPh_3)	physisorbed	n-type	80
Mechanical Exfoliation	7,7,8,8-tetracyanoquinodimethane (TCNQ)	physisorbed	p-type	62
Mechanical Exfoliation	Nicotinamide adenine dinucleotide (NADH)	physisorbed	n-type	62
Mechanical Exfoliation	Benzyl Viologen (BV)	physisorbed	n-type	75
Mechanical Exfoliation	-NH_2 terminated thiol; mercaptoethylamine (MEA)	chemisorbed	n-type	71
Mechanical Exfoliation	-CF_3 terminated thiol; 1H,1H,2H,2H-perfluorodecanethiol (FDT)	chemisorbed	p-type	71
Mechanical Exfoliation	Alkanethiol	chemisorbed	Red-shifted PL	76
Chemical Exfoliation	L-cysteine	physisorbed	Oxidized dopant	64
Chemical Exfoliation	Organohalide: 2-iodo-acetamide and 2-iodo-methane	chemisorbed	Strong PL in 1T-MoS_2	58
Chemical Exfoliation	thiol molecules: p-mercaptophenol, thiophenol, 1-propanethiol, 1-nonanethiol, 1-dodecanethiol	chemisorbed	Red-shifted PL	72
Chemical and Liquid Phase Exfoliation	Aryl diazonium salts	chemisorbed	n-type	73
Liquid Phase Exfoliation	graphene oxide	physisorbed	p-type	78
Chemical Vapour Deposition	Graphene quantum dots	physisorbed	n-type	77
Chemical Vapour Deposition	4-fluorobenzyl mercaptan	chemisorbed	p-type	70
Chemical Vapour Deposition	Bis(trifluoromethane) sulfonimide (TFSI)	physisorbed	Healing V_S	74
Chemical Vapour Deposition	Gas adsorbate; O_2 and H_2O	chemisorbed	p-type	79

1.5 Outline of Thesis

This thesis is divided into two main parts focusing on two 2D materials, namely MoS_2 and graphene. In each part, with our contribution we address the following specific aims:

- Prepare a high quality 2D material.
- Probe the 2D nanosheets with spectroscopic and microscopy techniques to characterize their properties.
- Control the properties of the 2D material.

In the next chapter, ***Chapter 2***, we provide the experimental details relevant to the work described in this thesis, concerning both the preparation and the characterization techniques employed. CVD as the synthesis method to obtain MoS_2 and graphene will be illustrated. Then we explain the spectroscopic and microscopic characterization tools, namely X-ray photoelectron spectroscopy (XPS), Raman, infrared and photoluminescence (PL) spectroscopy, atomic force microscopy (AFM), scanning electron microscopy (SEM), transmission electron microscopy (TEM), contact angle, X-Ray diffraction (XRD) and transport measurements. Characteristic results for graphene or MoS_2 will also be presented for some techniques.

Chapter 3 is dedicated to the growth of MoS_2 by CVD. This technique is the best option for obtaining large crystalline domains of MoS_2. Many reports[82] on SL-MoS_2 growth by CVD demonstrate that this low-cost production method affords a high reproducibility and that single crystalline domains can be obtained if the nucleation density is low, which in turn depends on the CVD parameters including type of substrate, precursors, heating temperature and the CVD geometry. However, only few studies have been done to optimize the CVD geometry. In the study reported here, we propose an alternative approach in which, by putting the source material in a quartz cup placed several mm upstream of the substrate, we obtain a continuous film of single layer MoS_2 fully covering the substrate in the region close to the molybdenum precursor. Our results demonstrate that this geometry produces a gradient in MoO_3

vapour concentration during the growth process, which is highest in the edge region of the substrate closest to the Mo source and lower further away from the edge, where separate MoS_2 flakes are formed. The as-grown samples were characterized by AFM, SEM and TEM for what concerns the morphology and structure and by XPS to learn about surface stoichiometry of the obtained nanosheets. We used PL and Raman spectroscopy to verify the band gap and vibrational fingerprint of SL-MoS_2. Last but not least, to determine the mobility, devices were made with MoS_2 flake as active material.

In ***Chapter 4***, we present a study of the intrinsic defects of MoS_2 grown as described in the previous chapter. We first identified different types of defects by X-ray photoelectron spectroscopy and then monitored how these defect fingerprint peaks changed upon thermal annealing and surface functionalization. We also characterized our samples by FTIR to verify the presence of the attached molecules via their vibrational fingerprint and by PL to study the electronic properties of MoS_2 upon functionalization.

In ***Chapter 5***, we report our study on the control of the photoluminescence properties of MoS_2 by surface functionalization. We first used a derivative of TCNQ, well-known p-dopant for low dimensional materials, to which a thiol group had been added. The thiol acts as anchoring group, which heals the S vacancies in MoS_2. The PL results indicate that the chemisorbed molecules efficiently increase the PL intensity via charge transfer. The successful covalent functionalization was confirmed by XPS and the quality of MoS_2 before and functionalization was monitored by Raman spectroscopy. We also demonstrated that an n-type thiol-functionalized molecules quench the PL intensity and thereby confirm that charge transfer is at the origin of the PL intensity variations induced by surface functionalization.

In ***Chapter 6***, we focus on the application of the oxidized graphene as an anti-icing coating. Recently, fluorinated graphene was demonstrated to delay ice formation for more than 30 minutes at subzero temperatures.[83] However, the defect-poor graphene in that study was obtained by CVD on a metallic coating. This approach yields non-transparent coatings and is therefore not suitable for camera lenses. In the study

reported here, we describe an up-scalable method for an anti-icing coating based on graphene oxide prepared using Langmuir-Schaefer deposition.

References

1 *U.S. Pat. 1,745,175*, 1930, 28–31.
2 G. E. Moore, *Electronics*, 1965, **38**, 114–117.
3 K. S. Novoselov, A. K. Geim, S. V. Morozov, D. Jiang, Y. Zhang, S. V. Dubonos, I. V. Grigorieva and A. A. Firsov, *Science (80-.).*, 2004, **306**, 666–669.
4 A. K. Geim and K. S. Novoselov, *Nat. Mater.*, 2007, **6**, 183–191.
5 Y.-C. Chen, T. Cao, C. Chen, Z. Pedramrazi, D. Haberer, D. G. de Oteyza, F. R. Fischer, S. G. Louie and M. F. Crommie, *Nat. Nanotechnol.*, 2015, **10**, 156–60.
6 N. Schmidt, 2019.
7 Y. Zhang, J. Ye, Y. Matsuhashi and Y. Iwasa, *Nano Lett.*, 2012, **12**, 1136–1140.
8 M. P. K. Sahoo, J. Wang, Y. Zhang, T. Shimada and T. Kitamura, *J. Phys. Chem. C*, 2016, **120**, 14113–14121.
9 Y. Zhang, H. Li, L. Wang, H. Wang, X. Xie, S.-L. Zhang, R. Liu and Z.-J. Qiu, *Sci. Rep.*, 2015, **5**, 7938.
10 P. R. Wallace, *Phys. Rev.*, 1947, **71**, 622–634.
11 H. P. Boehm, A. Chemie, D. U. Miinchen, K. Words and A. Nanoparticles, 1991, 581–584.
12 B. Kooi, G. Van Tendeloo, F. Zerbetto, M. Quintana, S. Bals, M. Calvaresi, K. Spyrou, P. Rudolf, M. Prato and M. Grzelczak, *J. Am. Chem. Soc.*, 2012, **134**, 13310–13315.
13 H. W. Kroto, J. R. Heath, S. C. O'Brien, R. F. Curl and R. E. Smalley, *Nature*, 1985, **318**, 162–163.
14 X. Chen, W. Wei, W. Lv, F. Su, Y. He and B. Li, *Chem. Commun.*, 2012, **48**, 5904–5906.
15 Dhiraj Prasai, J. C. Tuberquia, R. R. Harl, G. K. Jennings and K. I. Bolotin, *ACS Nano*, 2012, **6**, 1102–1108.
16 H. Shen, L. Zhang, M. Liu and Z. Zhang, *Theranostics*, 2012, **2**, 283–294.
17 Q. Tannock, *Nat. Mater.*, 2012, **11**, 2–5.
18 L. Zou, L. Wang, Y. Wu, C. Ma, S. Yu and X. Liu, *J. Data Inf. Sci.*, 2018, **3**, 82–100.
19 S. Garaj, W. Hubbard, a Reina, J. Kong, D. Branton and J. a Golovchenko, *Nature*, 2010, **467**, 190–193.
20 G. Eda and M. Chhowalla, *Nano Lett.*, 2009, **9**, 814–818.
21 J. H. Jung, D. S. Cheon, F. Liu, K. B. Lee and T. S. Seo, *Angew. Chemie Int. Ed.*, 2010, **49**, 5708–5711.
22 C. N. R. Rao, K. Gopalakrishnan and U. Maitra, *ACS Appl. Mater. Interfaces*, 2015, **7**, 7809–7832.
23 R. A. W. Dryfe and M. A. Bissett, *ACS Nano*, 2017, **11**, 11082–11090.
24 B. Y. Zhu, S. Murali, W. Cai, X. Li, J. W. Suk, J. R. Potts and R. S. Ruoff, *Adv. Mater.*, 2010, **22**, 3906–3924.
25 M. Chhowalla, H. S. Shin, G. Eda, L.-J. Li, K. P. Loh and H. Zhang, *Nat. Chem.*, 2013, **5**, 263–75.
26 C. R. Dean, A. F. Young, I. Meric, C. Lee, L. Wang, S. Sorgenfrei, K. Watanabe, T. Taniguchi, P. Kim, K. L. Shepard and J. Hone, *Nat. Nanotechnol.*, 2010, **5**, 722–726.
27 A. Ayari, E. Cobas, O. Ogundadegbe and M. S. Fuhrer, *J. Appl. Phys.*, 2007, **101**, 014507.
28 Q. H. Wang, K. Kalantar-Zadeh, A. Kis, J. N. Coleman and M. S. Strano, *Nat. Nanotechnol.*, 2012, **7**, 699–712.
29 M. Osada and T. Sasaki, *Adv. Mater.*, 2012, **24**, 210–228.
30 D. Voiry, A. Mohite and M. Chhowalla, *Chem. Soc. Rev.*, 2015, **44**, 2702–12.
31 J. Zhou, J. Lin, X. Huang, Y. Zhou, Y. Chen, J. Xia, H. Wang, Y. Xie, H. Yu, J. Lei, D. Wu, F. Liu, Q. Fu, Q. Zeng, C. Hsu, C. Yang, L. Lu and T. Yu, *Nature*, 2018, **556**, 355–60.
32 X. Duan, C. Wang, A. Pan, R. Yu and X. Duan, *Chem. Soc. Rev.*, 2015, **44**, 8859–8876.
33 I. Song, C. Park and H. C. Choi, *RSC Adv.*, 2015, **5**, 7495–7514.
34 R. S. Sundaram, M. Engel, A. Lombardo, R. Krupke, A. C. Ferrari, P. Avouris and M. Steiner,

Nano Lett., 2013, **13**, 1416–1421.
35 K. Gołasa, M. Grzeszczyk, K. P. Korona, R. Bożek, J. Binder, J. Szczytko, a. Wysmołek and a. Babiński, *Acta Phys. Pol. A*, 2013, **124**, 849–851.
36 B. Peng, P. K. Ang and K. P. Loh, *Nano Today*, 2015, **10**, 128–137.
37 G. Li, D. Zhang, Q. Qiao, Y. Yu, D. Peterson, A. Zafar, R. Kumar, S. Curtarolo, F. Hunte, S. Shannon, Y. Zhu, W. Yang and L. Cao, *J. Am. Chem. Soc.*, 2016, **138**, 16632–16638.
38 M. Chhowalla, D. Voiry, J. Yang, H. S. Shin and K. P. Loh, *MRS Bull.*, 2015, **40**, 585–591.
39 A. Splendiani, L. Sun, Y. Zhang, T. Li, J. Kim, C.-Y. Chim, G. Galli and F. Wang, *Nano Lett.*, 2010, **10**, 1271–1275.
40 C. Kittel, *Wiley Sons, New York, NY*.
41 A. Kumar and P. K. Ahluwalia, *Eur. Phys. J. B*, 2012, **85**, 18–22.
42 K. F. Mak and J. Shan, *Nat. Photonics*, 2016, **10**, 216–226.
43 H. Zeng and X. Cui, *Chem. Soc. Rev.*, 2015, **44**, 2629–2642.
44 K. F. Mak, C. Lee, J. Hone, J. Shan and T. F. Heinz, *Phys. Rev. Lett.*, 2010, **105**, 136805.
45 B. Radisavljevic, A. Radenovic, J. Brivio, V. Giacometti and A. Kis, *Nat. Nanotechnol.*, 2011, **6**, 147–150.
46 Y. Lin, X. Ling, L. Yu, S. Huang, A. L. Hsu, Y. H. Lee, J. Kong, M. S. Dresselhaus and T. Palacios, *Nano Lett.*, 2014, **14**, 5569–5576.
47 Y. Cai, H. Zhou, G. Zhang and Y.-W. Zhang, *Chem. Mater.*, 2016, **28**, 8611–8621.
48 K. F. Mak, K. He, C. Lee, G. H. Lee, J. Hone, T. F. Heinz and J. Shan, *Nat. Mater.*, 2013, **12**, 207–211.
49 E. J. Sie, A. J. Frenzel, Y. H. Lee, J. Kong and N. Gedik, *Phys. Rev. B - Condens. Matter Mater. Phys.*, 2015, **92**, 1–8.
50 D. Y. Qiu, F. H. Da Jornada and S. G. Louie, *Phys. Rev. Lett.*, 2013, **111**, 1–5.
51 D. Liu, Y. Guo, L. Fang and J. Robertson, *Appl. Phys. Lett.*, 2013, **103**, 183113.
52 Y. Lee, S. Park, H. Kim, G. H. Han, Y. H. Lee and J. Kim, *Nanoscale*, 2015, **7**, 11909–11914.
53 G. Deokar, D. Vignaud, R. Arenal, P. Louette and J. F. Colomer, *Nanotechnology*, 2016, **27**, 10.
54 X. Zeng, H. Hirwa, S. Metel, V. Nicolosi and V. Wagner, *Solid. State. Electron.*, 2018, **141**, 58–64.
55 H. Nan, Z. Wang, W. Wang, Z. Liang, Y. Lu, Q. Chen, D. He, P. Tan, F. Miao, X. Wang, J. Wang and Z. Ni, *ACS Nano*, 2014, **8**, 5738–5745.
56 Z. Yu, Y. Pan, Y. Shen, Z. Wang, Z.-Y. Ong, T. Xu, R. Xin, L. Pan, B. Wang, L. Sun, J. Wang, G. Zhang, Y. W. Zhang, Y. Shi and X. Wang, *Nat. Commun.*, 2014, **5**, 5290.
57 W. Zhou, X. Zou, S. Najmaei, Z. Liu, Y. Shi, J. Kong, J. Lou, P. M. Ajayan, B. I. Yakobson and J. C. Idrobo, *Nano Lett.*, 2013, **13**, 2615–2622.
58 S. Haldar, H. Vovusha, M. K. Yadav, O. Eriksson and B. Sanyal, *Phys. Rev. B*, 2015, **92**, 235408.
59 D. Voiry, A. Goswami, R. Kappera, C. D. C. C. E. Silva, D. Kaplan, T. Fujita, M. Chen, T. Asefa, M. Chhowalla, C. De Carvalho Castro e Silva, D. Kaplan, T. Fujita, M. Chen, T. Asefa and M. Chhowalla, *Nat. Chem.*, 2014, **7**, 45–49.
60 K. C. Knirsch, N. C. Berner, H. C. Nerl, C. S. Cucinotta, Z. Gholamvand, N. McEvoy, Z. Wang, I. Abramovic, P. Vecera, M. Halik, S. Sanvito, G. S. Duesberg, V. Nicolosi, F. Hauke, A. Hirsch, J. N. Coleman and C. Backes, *ACS Nano*, 2015, **9**, 6018–6030.
61 C. Backes, N. C. Berner, X. Chen, P. Lafargue, P. LaPlace, M. Freeley, G. S. Duesberg, J. N. Coleman and A. R. McDonald, *Angew. Chemie Int. Ed.*, 2015, **54**, 2638–2642.
62 R. J. Smith, P. J. King, M. Lotya, C. Wirtz, U. Khan, S. De, A. O'Neill, G. S. Duesberg, J. C. Grunlan, G. Moriarty, J. Chen, J. Wang, A. I. Minett, V. Nicolosi and J. N. Coleman, *Adv. Mater.*, 2011, **23**, 3944–3948.
63 S. Mouri, Y. Miyauchi and K. Matsuda, *Nano Lett.*, 2013, **13**, 5944–5948.
64 Q. Ding, K. J. Czech, Y. Zhao, J. Zhai, R. J. Hamers, J. C. Wright and S. Jin, *ACS Appl. Mater. Interfaces*, 2017, **9**, 12734–12742.

65 X. Chen, N. C. Berner, C. Backes, G. S. Duesberg and A. R. McDonald, *Angew. Chemie - Int. Ed.*, 2016, **55**, 5803–5808.

66 D. M. Sim, M. Kim, S. Yim, M. J. Choi, J. Choi, S. Yoo and Y. S. Jung, *ACS Nano*, 2015, **9**, 12115–12123.

67 J. I. Paredes, J. M. Munuera, S. Villar-Rodil, L. Guardia, M. Ayán-Varela, A. Pagán, S. D. Aznar-Cervantes, J. L. Cenis, A. Martínez-Alonso and J. M. D. Tascón, *ACS Appl. Mater. Interfaces*, 2016, **8**, 27974–27986.

68 Y. Yin, J. Han, Y. Zhang, X. Zhang, P. Xu, Q. Yuan, L. Samad, X. Wang, Y. Wang, Z. Zhang, P. Zhang, X. Cao, B. Song and S. Jin, *J. Am. Chem. Soc.*, 2016, **138**, 7965–7972.

69 R. Kurapati, L. Muzi, A. P. R. de Garibay, J. Russier, D. Voiry, I. A. Vacchi, M. Chhowalla and A. Bianco, *Adv. Funct. Mater.*, , DOI:10.1002/adfm.201605176.

70 J. Choi, H. Zhang and J. H. Choi, *ACS Nano*, 2016, **10**, 1671–1680.

71 Z. Li, R. Ye, R. Feng, Y. Kang, X. Zhu, J. M. Tour and Z. Fang, *Adv. Mater.*, 2015, **27**, 5235–5240.

72 H. M. Oh, H. Jeong, G. H. Han, H. Kim, J. H. Kim, S. Y. Lee, S. Y. Jeong, S. Jeong, D. J. Park, K. K. Kim, Y. H. Lee and M. S. Jeong, *ACS Nano*, 2016, **10**, 10446–10453.

73 H. M. Oh, G. H. Han, H. Kim, J. J. Bae, M. S. Jeong and Y. H. Lee, *ACS Nano*, 2016, **10**, 5230–5236.

74 K. Heo, S. Jo, J. Shim, D. Kang, J. Kim and J. Park, *ACS Appl. Mater. Interfaces*, 2018, **10**, 32765–32772.

75 Q. Ding, K. J. Czech, Y. Zhao, J. Zhai, R. J. Hamers, J. C. Wright and S. Jin, *ACS Appl. Mater. Interfaces*, 2017, **9**, 12734–12742.

76 D. M. Sim, M. Kim, S. Yim, M. J. Choi, J. Choi, S. Yoo and Y. S. Jung, *ACS Nano*, 2015, **9**, 12115–12123.

77 E. P. Nguyen, B. J. Carey, J. Z. Ou, J. Van Embden, E. Della Gaspera, A. F. Chrimes, M. J. S. Spencer, S. Zhuiykov, K. Kalantar-Zadeh and T. Daeneke, *Adv. Mater.*, 2015, **27**, 6225–6229.

78 X. S. Chu, A. Yousaf, D. O. Li, A. A. Tang, A. Debnath, D. Ma, A. A. Green, E. J. G. Santos and Q. H. Wang, *Chem. Mater.*, 2018, **30**, 2112–2128.

79 S. Roy, W. Choi, S. Jeon, D. H. Kim, H. Kim, S. J. Yun, Y. Lee, J. Lee, Y. M. Kim and J. Kim, *Nano Lett.*, 2018, **18**, 4523–4530.

80 D. Kiriya, M. Tosun, P. Zhao, J. S. Kang and A. Javey, *J. Am. Chem. Soc.*, 2014, **136**, 7853–6.

81 K. Cho, M. Min, T. Y. Kim, H. Jeong, J. Pak, J. K. Kim, J. Jang, S. J. Yun, Y. H. Lee, W. K. Hong and T. Lee, *ACS Nano*, 2015, **9**, 8044–8053.

82 H. F. Liu, S. L. Wong and D. Z. Chi, *Chem. Vap. Depos.*, 2015, **21**, 241–259.

83 N. Akhtar, G. Anemone, D. Farias and B. Holst, *Carbon N. Y.*, 2019, **141**, 451–456.